Chapter-6

Fluorescent CNDs from Asparagus racemosus and their various applications

6.1 Introduction

Asparagus racemosus (AR) has exhibited a wide range of biological activities and hence various efforts have been made to develop its pharmaceutical formulations [Majumdar *et al.,* 2021, Pandey *et al.,* 2022]. Recent breakthroughs in nano-biotechnologies have increased the availability of nanomaterials of various sizes and structures, opening up many new possibilities for developing new fluorescent nano-probes. Bio-imaging, therapeutic delivery, metal ion detection, and other fields have already employed carbon nanodots (CNDs) as potential nano-probes [Dordevic *et al.,* 2022]. CNDs generated from plants have shown substantial promise in these fields, among others. CNDs are the emerging carbogenic nanomaterials that have sparked much interest in recent years because of their many benefits, including excellent solubility, photobleaching resistance, minimal cytotoxicity, and strong biocompatibility. Chemical doping in nanomaterials can alter the materials' physical properties and chemical reactivity [Khan *et al.,* 2021].

Here, to overcome the above issues, we have reported the development of fluorescent CNDs derived from AR. We have incorporated carrageenan and polyethyleneimine (PEI) as doping agents to improve the fluorescence quantum yield and biophysical aspects of CNDs. Apart from sensing As^{3+} and Ag^{+}, the current study focuses on the inhibitory effect on cancer cell proliferation against breast (MDA-MB-231) and cervical (SiHa) cancer

cells. *In-vivo* toxicity evaluation of CNDs has also been carried out in swiss albino mice. To the best of our knowledge, this is the first report demonstrating the fabrication of carbon nanodots using *Asparagus racemosus* and its potential applications in biomedical and environmental analysis.

6.2 Experimental section

6.2.1 Materials

All the procured chemicals, reagents, and solvents were of analytical grade. MTT (3-(4, 5-dimethylthiazol-2-yl)-2, 5-diphenyltetrazolium bromide), DAPI (4′,6-diamidino-2-phenylindole), and DPPH (1, 1-diphenyl-2-picrylhydrazyl) were purchased from Sigma-Aldrich Co. LLC. *Asparagus racemosus* (AR) roots were collected from the Indian Institute of Technology (BHU) campus and authenticated using DNA fingerprinting with the matK gene as per the previously reported method [White *et al.,* 1990]. A certified taxonomist also authenticated the plant, and the specimen has been deposited in the herbarium with specimen number 2021/5 for future reference.

6.2.2 Fabrication of CNDs from *Asparagus racemosus* (AR)

To prepare an aqueous extract, 20 g of fresh roots of AR were washed thoroughly in distilled water and dried to remove moisture. The dried root powder was then subjected to 96 h maceration using 200 mL distilled water with intermittent heating & stirring. CNDs (ARCD and ARCCD) were synthesized via the hydrothermal treatment of aqueous fractions of AR roots as represented in Scheme **6.1**. ARCD was synthesized by subjecting aqueous extract at 160^{o}C for 8 h into a teflon-lined hydrothermal autoclave. ARCD was

then centrifuged for 15 min at 12000 rpm. ARCD was further purified using a membrane syringe filter (0.22 μm).

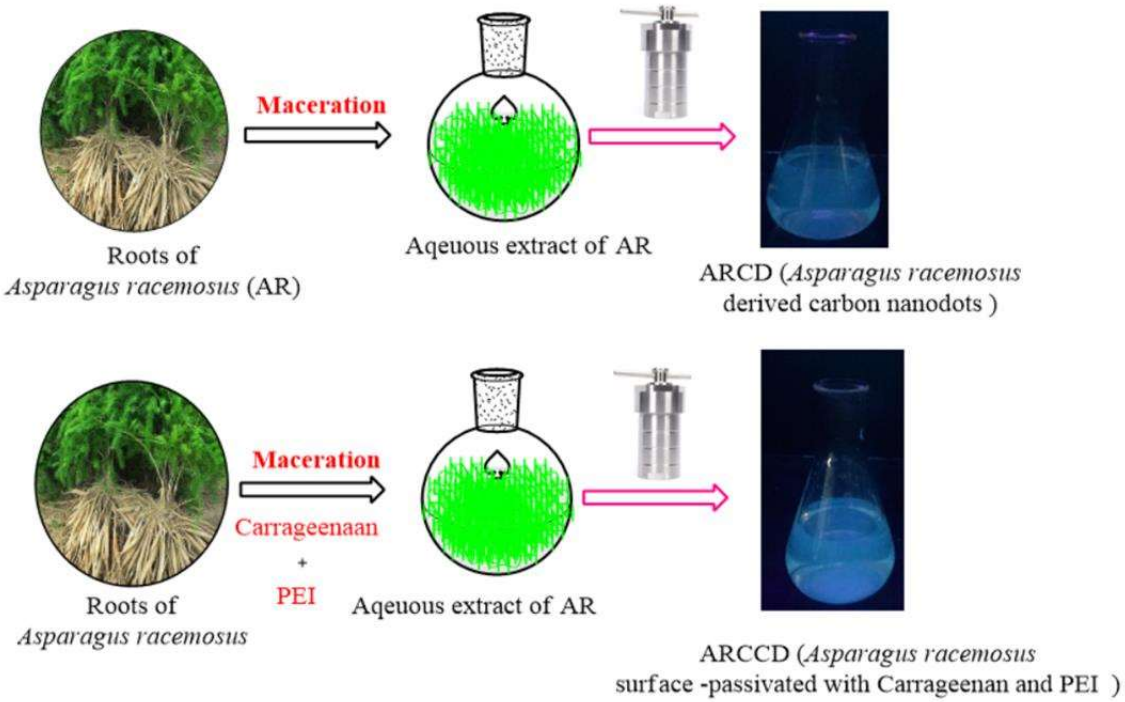

Scheme 6.1 Synthetic scheme for the preparation of ARCD and ARCCD by hydrothermal method.

To further improve the quantum yield, ARCCD was synthesized by subjecting the AR extract (10 g) and a 1:1 ratio of carrageenan (CAR) and polyethyleneimine (PEI) mixture to hydrothermal treatment at 160°C for 8 h in a Teflon-lined hydrothermal autoclave. ARCCD was then centrifuged for 15 min at 12000 rpm. ARCCD was further purified using a membrane syringe filter (0.22 μm). For further characterization and biological evaluations, ARCD and ARCCD were stored at 4°C.

6.2.3 Characterization, optical properties and stability studies

The fabricated CNDs has been characterized to study their size, morphology, fluorescence properties, surface functional groups, crystallinity, elemental composition, stability and quantum yield using different techniques. The detail procedures for the metal sensing by CNDs are provided in chapter **3**.

A previously described integrating sphere method was used to measure the quantum yield of CNDs. First, the CNDs' aqueous solution was diluted to keep the absorption intensity below 0.1 in the 10 mm fluorescence cuvette at the excitation wavelength (350 nm). Then it was placed in an integrating sphere (QuantaPhi-2, HORIBA) and excited with 350 nm light from the Xe-lamp. Fluorescence spectra of CNDs were recorded at 340–360 nm (for excitation peak) and 375–575 nm (for emission peak). Meanwhile, we observed the same fluorescence spectra of pure water under identical conditions. Finally, we calculated the quantum yield using in-built software. The average quantum yield value was computed after three rounds of experiments.

6.2.4 Applications of ARCD and ARCCD

6.2.4.1 Sensing of environmentally and biologically relevant metal ions

The metal ion sensing ability of the ARCD and ARCCD was evaluated as per the previously reported methods with certain modifications [Hu *et al.,* 2021]. The detail procedures for the metal sensing by ARCD and ARCCD are provided in chapter **3**.

6.2.4.2 Cytotoxicity studies

MTT assay was employed to evaluate the cytotoxic effect of ARCD and ARCCD on MDA-MB-231, SiHa, and HEK-293 cell lines as per the previously reported method

with slight modifications [Naik *et al*., 2020]. The detail procedures are provided in chapter **3**.

Morphology detection of cells using phase-contrast microscopy

To examine ARCD and ARCCD-induced morphological changes in MDA-MB-231 and HEK-293 cells, the cells were plated and incubated overnight. Subsequently, the cells were exposed to various doses of ARCD and ARCCD for 24 hours. After the respective treatment period, the cells were washed and observed under the phase-contrast microscope at 10X magnification [Khandelwal *et al.,* 2019].

Cellular uptake studies

DAPI labeling was used to look at morphological alterations in the nuclei of HEK-293 and MDA-MB-231 cells. Both cells (10^4-10^5/well) were seeded into a 96-well plate individually, grew for 24 hours, and exposed to various doses of ARCD and ARCCD for 24 hours. Next, the cells were fixed with paraformaldehyde and permeabilized with methanol (100 µL/well) for 30 minutes at -20°C. Subsequently, the cells were washed and stained with DAPI (2 µg/mL) at room temperature and photographed at 20X magnification under a fluorescence microscope [Khandelwal *et al.,* 2019].

Western blot assay

To examine the effect of ARCD and ARCCD on the expression of proteins involved in apoptosis, western blotting was performed [Minocha *et al.,* 2022]. After treating the cells with various doses of ARCD and ARCCD, the protein concentration was determined by Bradford assay, and the total protein (40 µg) was separated on 12%

SDS-PAGE. The proteins were transferred onto nitrocellulose membranes after 120 minutes of electrophoresis at 100 V and blocked for 1 hour in skimmed milk. The membranes were incubated overnight at 4°C against Bax, Bcl-2, and β-actin antibodies diluted at 1:1000 dilution. The blots were washed 2-3 times with TBST and probed with secondary antibodies at 1:1000 dilution. The blots were rewashed and imaged using a ChemiDoc MP Imaging System (BioRad).

6.2.4.3 Viability studies using MDR bacterial strains

The disk diffusion method with slight modifications was employed to perfrom the viability studies using nine different clinically isolated MDR bacterial strains, i.e., Gram-negative (*Enterobacter cloacae*, *Acinetobacter baumannii*, *Pseudomonas aeruginosa*, *Escherichia coli*, *Klebsiella pneumonia*, and *Aeromonas hydrophila* and Gram-positive (*Enterococcus faecalis*, *Staphylococcus aureus* and Methicillin-Resistant *Staphylococcus aureus*) with 20 µL of 30.00 mg/mL and 40.00 mg/mL ARCD and ARCCD, respectively. Other details have been provided in Chapter **3**.

6.2.4.4 Free radical scavenging potential

The radical scavenging ability of ARCD and ARCCD at different concentrations of 0-250 µg/mL was determined using a modified DPPH assay. The detail procedures for the free radical scavenging potential of CNDs are provided in chapter **3**.

6.2.4.5 In-vivo toxicity evaluation

CNDs are expected not to induce severe adverse effects in animals to be used in therapeutic settings. CNDs were tested *in-vivo* on mice for 14 days to see if they were biocompatible. Routine blood tests, blood biochemistry assays, and histological

examinations for the control group (Phosphate Buffered Saline group), ARCD, and ARCCD groups were performed to examine the biosafety of the CNDs.

On day 0, the CNDs were dispersed in PBS to make different concentration dispersions (1 and 2 mg/kg BW for ARCD, 4 and 8 mg/kg BW for ARCCD) and administered intraperitoneal injection. Mice in the control group were administered with PBS. All of the experimental animals survived the experiment, and their body weight changes were identical to those of the control group. On the 14th day, blood was obtained from the mice, and routine biochemical and hematological assays were done as described in chapter **3**.

6.2.5 Statistical analysis

The data is presented as a mean ± standard deviation (SD). One-way ANOVA was used to perform the statistical studies (GraphPad Prism Version 5.0). $p < 0.05$ was considered as a criterion for significance.

6.3 Results and discussion

6.3.1 Formation of ARCD and ARCCD

The collected plant was authenticated as *Asparagus racemosus* (AR) by DNA fingerprinting method using the matK gene. Figure **6.1** shows a PCR gel image with the matK gene. AR has been shown to inhibit DMBA-induced mammary carcinogenesis in rats. It has been called a Rasayana rasayana herb. The roots contain 9, 10-dihydro-1,5-dimethoxy-8-methyl-2,7-phenanthrene diol, an alkaloid known as asparagamine A, and saponins such as shatavarin I-IV, which have anticancer properties [Bopana *et al.,* 2007,

Bhutani *et al.,* 2010]. The aqueous extract contains various nitrogen and sulfur-containing phytoconstituents and biological macromolecules such as shatavarins, shatavaroside A, steroidal saponins, schidigerasaponin D5, immunoside, filiasparoside C, and asparanin A, shatavaroside B, etc. [Bhutani *et al.,* 2010].

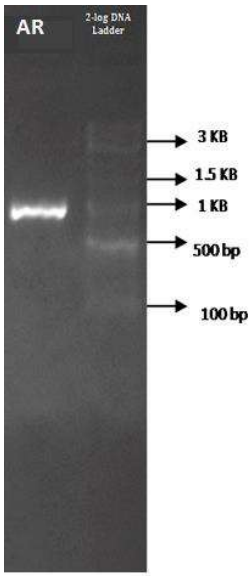

Figure 6.1. PCR gel image with matK gene.

Carrageenan is a natural sulfated polymer with linear anionic heteropolysaccharides extracted from red algae and sold commercially. They are made up of long linear d-galactose and d-anhydrogalactose chains containing ester sulfates [Emam *et al.,* 2021]. PEI is a functional polycationic polymer with primary, secondary, and tertiary amine groups that is water-soluble [Rdest *et al.,* 2020]. Hence, ARCD were surface passivated with carrageenan, which is rich in sulfur, and PEI, rich in nitrogen, as doping agents to enhance the fluorescence quantum yield.

6.3.2. Characterization of ARCD and ARCCD

The ARCDs were uniform, monodispersed spheres with a size distribution of 2.7 to 6.2 nm, as seen in typical HR-TEM images of CNDs (Figure **6.2 a**). The average mean diameter of ARCD is roughly 4.61 ±0.33 nm. The ARCCD size distribution, on the other hand, ranges from 5.5 to 7.9 nm, with an average mean diameter of 6.31 ±0.33 nm (Figure **6.2 c**). The increasing size of ARCCD shows that carrageenan and polyethyleneimine molecules on their surface have been successfully passivated. C, O, and N elements were abundantly present in as-prepared CNDs, whereas S was poorly dispersed, according to the energy-dispersive X-ray spectroscopy study (EDX) (Figure **6.2 g**).

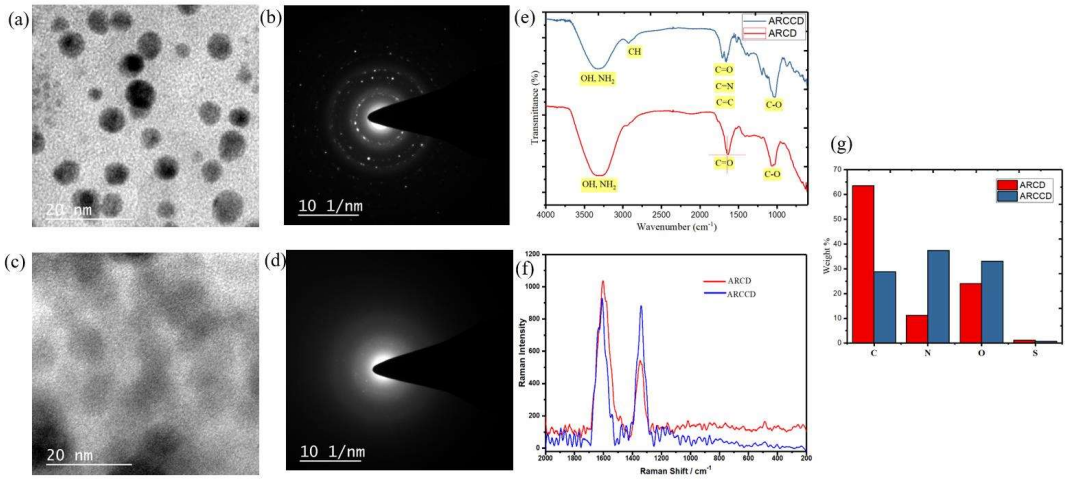

Figure 6.2. Morphology and Structure [a] HR-TEM image of ARCD at 20 nm resolution [b] Selected area electron diffraction pattern of ARCD [c] HR-TEM image of ARCCD at 20 nm resolution [d] Selected area electron diffraction pattern of ARCCD [e] FT-IR spectra of ARCD and ARCCD [f] Raman spectra of ARCD and ARCCD [g] Energy dispersive X-ray analysis (EDXA) of ARCD and ARCCD.

Furthermore, the SAED pattern of ARCD and ARCCD, as shown in Figure **6.2 b** and **6.2 d** consist of a dispersed halo devoid of rings, demonstrating the amorphous and

polycrystalline character of the synthesized CNDs. The elemental abundance and composition of CNDs were determined using EDAX. EDS elemental mapping revealed the presence of oxygen (O), nitrogen (N), carbon (C), and sulfur (S) in modest amounts revealed by of CNDs, which can be associated with the presence of numerous functional groups on CNDs' surface. Higher C and O content and lower N content in ARCD and higher O, N content in ARCCD revealed that these CNDs mainly were made up of carbon, oxygen, and nitrogen-containing functional groups, with a few sulfur-containing functional groups.

FT-IR spectra was analyzed to study the chemical composition of as-synthesized CNDs (Figure **6.2 e**). Peaks at 3327.9 cm^{-1} and 2935.8 cm^{-1} were attributed to O-H/N-H stretching bands and C-H stretching vibrations, respectively. A peak at 1524.5 cm^{-1} corresponded to N-H deformation vibrations. C-O and C-O-C bonds' stretching and bending vibrations were attributed to peaks at 1118.7 cm^{-1} and 1040.6 cm^{-1}. In addition, the FT-IR spectrum of ARCCD exhibited the absorption peaks at 1662.6 cm^{-1} and 1714.1 cm^{-1}, attributed to stretching vibration of C=O, C=N, and C=C bonds. The FT-IR spectrum of ARCD exhibited a sharp absorption peak at 1644.0 cm^{-1}, corresponding to the stretching vibration of C=O. A modest absorption peak identifies the CS group at 675.6 cm^{-1}. Thus, the as-prepared CNDs were functionalized with carboxylic, hydroxyl, alkyl and aryl, amino, sulfur, and other groups produced from phytomolecules in *A. racemosus* after hydrothermal treatment, according to the results [Chen et al., 2021].

Raman analysis was used further to investigate the structural aspects of ARCD and ARCCD. The Raman spectra of ARCD and ARCCD are presented in Figure **6.2 f**. As expected for CNDs, the spectra show the existence of two peaks, attributed as the D band

(1350 cm^{-1}) and G band (1590 cm^{-1}). These D and G bands in Raman spectra provide information on sp^2 hybridization in CNDs. The ratio of the intensity of D band (I_D) to intensity of G band (I_G) (i.e., I_D/I_G) for ARCD and ARCCD was found to be 0.54 and 0.96, respectively, which yields a graphitization degree measurement [Mathew *et al.*, 2020]. The oxygenated and nitrogenized groups on the surface of CNDs are linked to these surface defects.

The chemical composition of the ARCD and ARCCD was studied using X-ray photoelectron spectroscopy (XPS). As shown in Figure **6.3 a** and **6.3 e**, XPS spectra of ARCD and ARCCD revealed four peaks related to carbon, nitrogen, oxygen, and sulfur atoms.

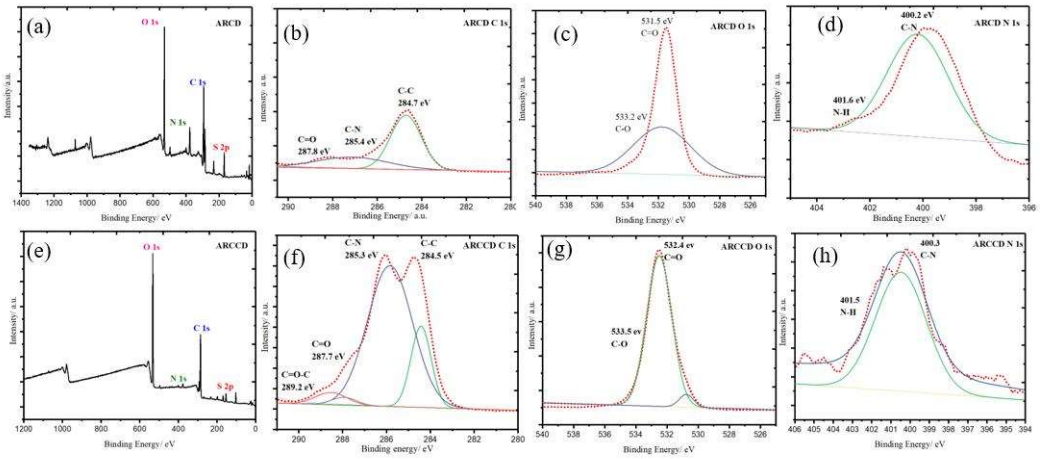

Figure 6.3. [a] XPS survey spectra of the ARCD [b] XPS high-resolution survey scan of C 1s, [c] N 1s and [d] O 1s region of the ARCD [e] XPS survey spectra of the ARCCD [f] XPS high-resolution survey scan of C 1s, [g] N 1s and [h] O 1s region of the ARCCD.

ARCD's high-resolution C 1s spectrum (Figure **6.3 b**) is split into three separate peaks. At 284.7eV, the primary and most crucial peak is related to C–C bonds. The second peak, at 285.4 eV, is attributed to C–N bonds, while the third peak, at 287.8 eV, is attributed to

C=O bonds. On the other hand, the high-resolution C 1s spectrum of the ARCCD (Figure **6.3 f**) is separated into four distinct peaks. At 284.5 eV, the first and most crucial component is related to C–C bonds. The second peak, at 285.3 eV, is assigned to C–N bonds, while the third peak, at 287.7 eV, is credited to C=O bonds, and the fourth peak, at 289.2 eV, is attributed to C–O bonds. The high-resolution XPS spectrum of N 1s for the ARCD is shown in Figure **6.3 c**. C–N and N–H bonds can be linked to the two different peaks at 400.2 and 401.6 eV, respectively. Similarly, the ARCCD's high-resolution N 1s XPS spectrum (Figure **6.3 g**) shows two unique peaks at 400.3 and 401.5 eV, attributed to C–N and N–H bonds, respectively. These peaks confirm the synthesis of nitrogen-containing CND during the hydrothermal process. The ARCD O 1s spectrum (Figure **6.3 d**) has two prominent peaks at 531.5 and 533.2 eV, corresponding to C=O and C–O bonds, respectively. The ARCCD O 1s spectrum (Figure **6.3 h**) has two prominent peaks at 532.4 and 533.5 eV, corresponding to C=O and C–O bonds, respectively. Sulfur is also responsible for the peak at 169.0 eV. The XPS results confirm the synthesis of O, N, and S doped CNDs.

ARCD displayed the bluish-green fluorescence with a quantum yield of 2.46% at 350 nm while carrying out QY determination using the integrating sphere method [Guo *et al.,* 2018]. Surface-passivation with a 1:1 ratio of carrageenan and polyethyleneimine enhanced the quantum yield even further, to 4.47%. It has been suggested that nitrogen doping could reduce the bandgap by moving down the carbon conduction band edge. Improvement in the quantum yield of CNDs upon passivation with suitable polymers may be due to the promotion of disorders in the carbon hexagonal rings by nitrogen boding to carbon which may generate additional luminous centres by trapping radiative electron-

hole pairs [Xu *et al.,* 2013, Bourlinos *et al.,* 2008]. However, the photoluminescent mechanism of CNDs is yet unknown; thus, more research into the specific impacts of doping nitrogen will be necessary.

6.3.3 Optical properties of ARCD and ARCCD

Hydrolysis, dehydration, breakdown, condensation, aromatization, and passivation are the most likely synthesis mechanisms for ARCD and ARCCD [Xia *et al.,* 2019, Liu *et al.,* 2019]. After the aromatic centres have been sculpted, the photoluminescent carbon cores emerge. The photoluminescence behavioral properties of such fluorescent carbon nanomaterials could be explained by interactions between the carbon core and surrounding chemical moieties and hybridization [Xia *et al.,* 2019, Liu *et al.,* 2019]. Many attempts have been undertaken to dope CNDs with heteroatoms such as nitrogen (N), sulfur (S), boron (B), phosphorous (P), and fluorine (F) to generate CNDs with various characteristics and broaden their applications [Du *et al.,* 2016]. A synthetic scheme of ARCD and ARCCD is provided in Scheme **6.1**.

UV–Visible and fluorescence spectroscopy were used to investigate the ground and excited optical properties of ARCD and ARCCD in an aqueous medium (Figure **6.4**). Peaks at 272 and 352 nm in the UV–Visible absorption spectra corresponded to π to π* and n to π* transitions in the carbon-carbon double bond and carbonyl bond, respectively (Figure **6.4 a**). At 465 nm, there is a second shoulder peak in the UV-Vis spectrum of ARCCD (Figure **6.4 b**), which is attributed to the surface or molecular center [Xu *et al.,* 2014]. When the sample was exposed to UV light, the CNDs fluoresced bluish-green. The photoluminescence properties of CNDs were investigated and presented in Figure

6.4 b. When excited at 350 nm, both ARCD and ARCCD exhibit significant fluorescence at 380 to 550 nm and a maximum peak around 450 nm.

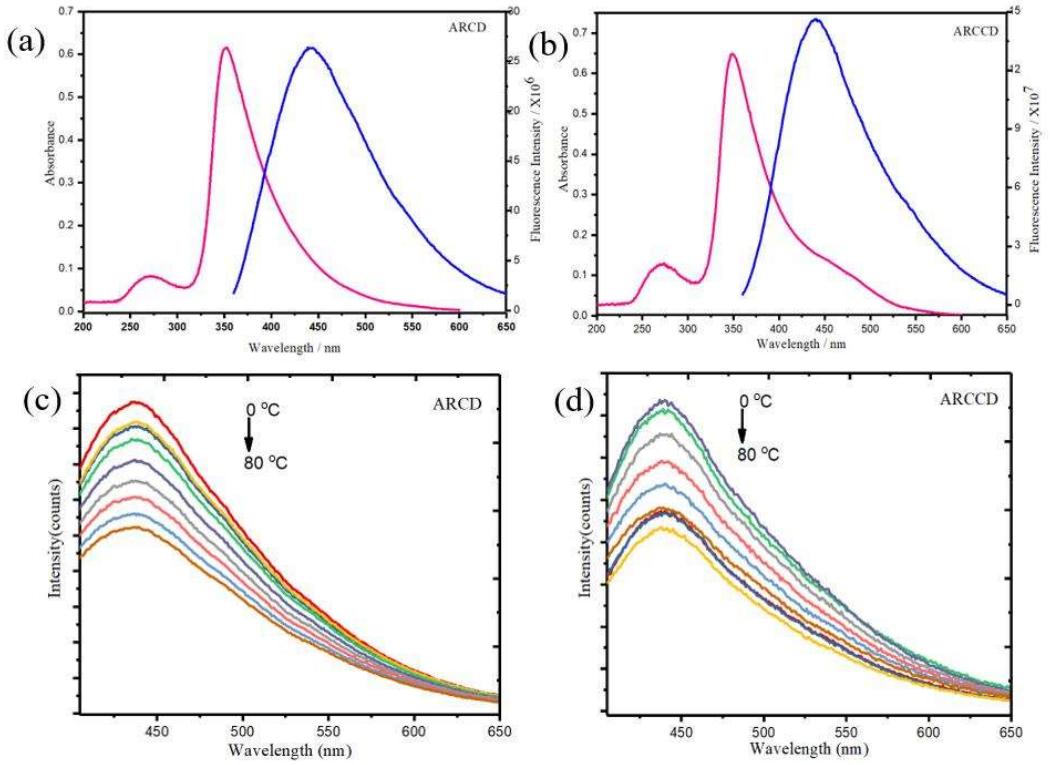

Figure 6.4. Absorption and fluorescence studies of ARCD and ARCCD. Absorption and fluorescence spectra of [a] ARCD [b] ARCCD. The fluorescence response of [c] ARCD d] ARCCD at different temperature are also shown.

The influence of temperature on the fluorescence of ARCD and ARCCD was also studied and shown in Figure **6.4 c** and **6.4 d**. Interestingly, the fluorescence intensity decreases with an increase in the temperature of the solution for both systems. Increased non-radiative deactivation pathways could explain the decrease in fluorescence with increased temperature [Kalytchuk *et al.,* 2017]. This temperature sensitivity of these CNDs can, in principle, be exploited as a temperature sensor.

6.3.4 Stability studies of ARCD and ARCCD

Determination of zeta potential (ZP) helps estimate surface charges which in turn assist in understanding the physical stability aspects of CNDs. A significant negative or positive ZP value implies better physical stability of CNDs owing to electrostatic repulsion between individual particles. ZP is useful in the prediction of particle agglomeration [Lunardi *et al.,* 2021]. As shown in Figure **6.5 a** and **6.5 b**, ARCD and ARCCD ZP in aqueous environments were -18.7 mV and -0.6 mV, respectively, which could be attributable to different hydroxyl, carbonyl, amine, carboxyl groups on the CNDs surface. The CNDs with negative surface charges are repelled in this scenario, preventing the particles from aggregating. ZP of -30 mV to +30 mV is thought to provide adequate repulsive force to achieve good physical colloidal stability [Lunardi *et al.,* 2021].

The thermal behaviour of CNDs was determined by weight loss as a function of temperature in a controlled environment, as shown in the thermogram (Figure **6.5 c**.) Initial weight loss of 4.45 % and 6.23 % at 100 °C was observed for ARCD and ARCCD, respectively, which may be due to the removal of molecules connected to CNDs via weak hydrogen bonds of water molecules. Further weight loss was observed at 600 °C (40.94 % for ARCD and 25.53 % for ARCCD) and 800 °C (60.32% for ARCD and 55.7% for ARCCD), owing to the organic functional groups' decomposition, implying CNDs' thermal stability up to 900 °C [Mewada *et al.,* 2013, Mehta *et al.,* 2014]. The curve levelled off beyond 900 °C, and just a tiny amount of burnt carbon remained. Earlier research has also observed these kinds of findings [Mewada *et al.,* 2013, Mehta *et al.,* 2014].

Under UV light at 365 nm, the photostability of ARCD and ARCCD was investigated. ARCD and ARCCD samples were irradiated to UV light for varying lengths of time and examined for changes in fluorescence property and intensity. As shown in Figure **6.5 d**, there was no photobleaching after 120 minutes of continuous exposure, and the fluorescence behavior was unaffected when viewed with the naked eye. When the UV-visible spectra of ARCD and ARCCD were examined before and after irradiation, the fluorescence intensity remained unchanged, indicating that optical characteristics and photostability were retained.

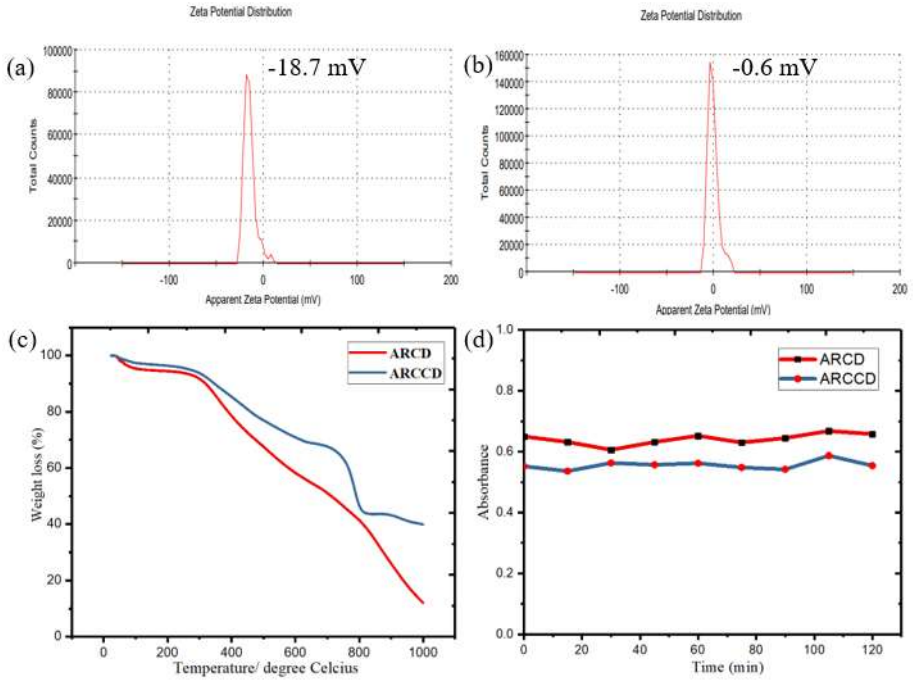

Figure 6.5.Stability studies of CNDs [a] Zeta potential of ARCD [b] Zeta potential of ARCCD [c] Thermo gravimetric analysis spectrum of ARCD and ARCCD [d] Photostability study of ARCD and ARCCD under UV illumination at a different time interval upto 120 min.

6.3.5 Applications of ARCD and ARCCD

ARCD and ARCCD has demonstrated utility in various biomedical and pharmaceutical domains such as metal sensing, cytotoxic potential, free radicals scavenging, viability studies against MDR bacterial strains, and *in-vivo* toxicity evaluation.

6.3.5.1 Metal sensing

Contamination of drinking water with arsenic (As^{3+}) is a significant issue worldwide. As^{3+} is the deadliest of the many types and is linked to various ailments, including high-risk lung or bladder cancer, skin damage, and cardiovascular difficulties [Mawia *et al.,* 2021]. The World Health Organization (WHO) recommends a threshold of 10 ppb (10 µg/L, 133 nM) in drinking water [Ezeh *et al.,* 2012]. Similarly, excessive Ag^{+} intake can cause cell toxicity, resulting in membrane damage and severe erythrocyte lysis [Asharani *et al.,* 2010]. Ag^{+} is thought to interact with various metabolites and enzymes, causing the enzymes to become inactive and causing health problems [Drake *et al.,* 2005]. The US EPA set the allowable Secondary Maximum Contaminant Level (SMCL) for Ag^{+} has been set at 0.1 mg/L by the US EPA [WHO, 2004]. As a result, As^{3+} and Ag^{+} ions must be analyzed in various biological and environmental samples. CNDs can assess the quality and safety of drinking water by assessing the quantity of these heavy metals.

As confirmed from FT-IR and elemental composition, different sets of functional groups are present on the surface of these CNDs, which interact differently with different metal ions. The fluorescence quenching was observed with an increase in the concentrations of As^{3+} and Ag^{+}, implying the adsorption of these ions onto the surface of CNDs, wherein

they promoted radiative recombination by acting as electron sinks and induced fluorescence quenching. The quenching effect was calculated by employing the Stern-Volmer (SV) equation, $F_0/F = 1+ K_{SV}$ [Q], where F_0 and F are the fluorescence intensities pre and post metal ions (quencher) addition, [Q] is the metal ion concentration and K_{SV} is the quenching constant [Zhou *et al.,* 2012].

Quenching may also be due to non-specific interactions between metal ions and functional groups such as carboxylic groups/amine groups of CNDs [Gong *et al.,* 2015]. In the presence of As^{3+} and Ag^{+} ions, the ARCD and ARCCD displayed the most quenching, indicating stronger selectivity toward sensing As^{3+} and Ag^{+} ions, respectively. With a gradual increase in the As^{3+} and Ag^{+} ion concentrations, the fluorescence intensity of ARCD and ARCCD decreased steadily in the metal sensitivity experiment. The non-radiative transfer of photoelectrons from multiple functionalized ARCD to the empty orbit of As^{3+} cations could explain the selective fluorescence quenching selectivity toward As^{3+} [Rajendran *et al.,* 2021, Ramezani *et al.,* 2018].

The selective fluorescence quenching toward Ag^{+}, on the other hand, could be owing to its chelation with ARCCD, which enables charge transfer from ARCCD's excited state to Ag^{+} [Jiang *et al.,* 2016]. Non-radiative charge recombination annihilation through an effective electron transfer process could cause luminescence quenching [Zheng *et al.,* 2015]. The surface of the ARCCD created by combining carrageenan and PEI was provided with many metal ion recognition sites, which was favourable for Ag^{+} detection. To study the detection selectivity of various metal cations by ARCD and ARCCD, the effect of the metal ions Ag^{+}, Na^{+}, K^{+}, Hg^{2+}, NH^{4+}, Cu^{2+}, Pb^{2+}, Al^{3+}, Bi^{3+} and As^{3+} at a concentration of 200µM was evaluated (Figure **6.6 a**). The limit of detection (LOD) of

CNDs on a selected metal ion in water was determined using: LOD=3σ/s, where σ is the standard deviation of F_0/F values and s is the slope of the linear line. The limit of detection (LOD) value is used to identify samples with low analyte levels [Zhu *et al.,* 2010].

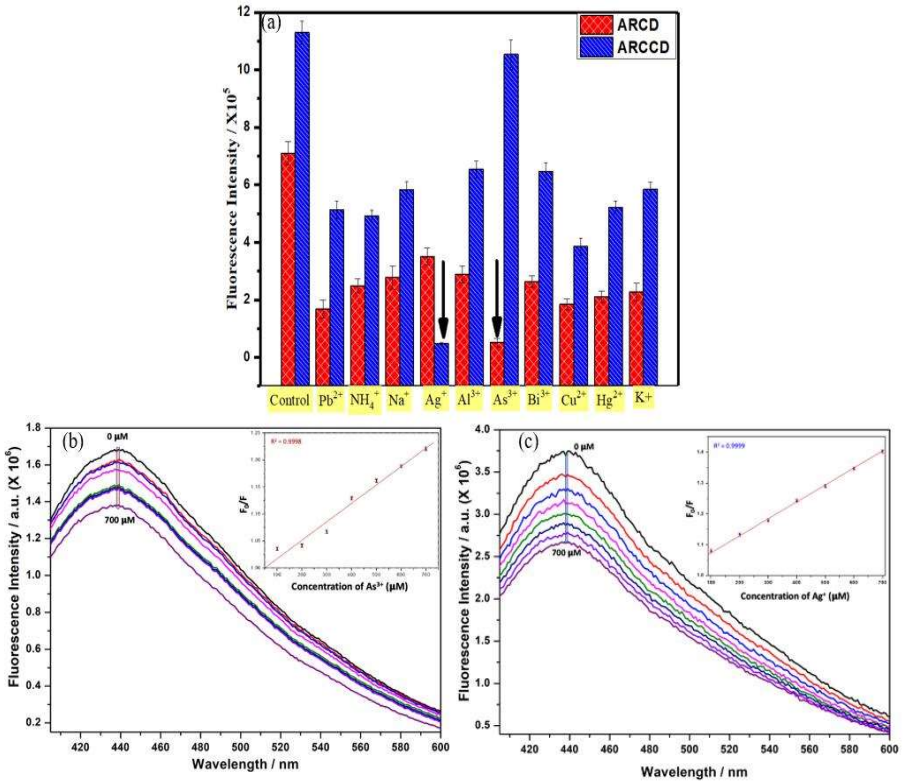

Figure 6.6. Fluorescence sensing of metal ions using ARCD and ARCCD. [a] Fluorescence responses of the ARCD and ARCCD toward various metal ions. The control represents the fluorescence response of the CNDs without any ion. [b] Fluorescence responses of the ARCD in the presence of different concentrations of As^{3+} [c] Fluorescence responses of the ARCCD in the presence of different concentrations of Ag^{+}. Inset of both [b] and [c] represents the linear relations between F0/F and the quencher concentration, for details, text is referred.

Accordingly, a sensitivity titration was performed under various As^{3+} and Ag^{+} concentrations ranging from 0 to 700 μM. With an increase in As^{3+} and Ag^{+} concentrations, the emission intensity of ARCD and ARCCD, respectively, decreased

gradually at 450nm, which revealed the potential of the present sensing probe for sensitive detection of As^{3+} and Ag^{+}. Figure **6.6 b** inset represents the relationship between F_0/F - 1 and As^{3+} concentrations, and Figure **6.6 c** inset displays the relationship between F_0/F -1 and Ag^{+} concentrations. As demonstrated in Figure **6.6 b** and **6.6 c**, a good linear relationship was obtained with a correlation coefficient (R^2) of 0.9998 for ARCD (LOD=0.227 µM) and R^2 of 0.9999 for ARCCD (LOD=0.052 µM). As a result, CNDs-based materials are likely to be useful for detecting various ionic chemicals.

6.3.5.2 Cytotoxicity assays against MDA-MB-231 and SiHa cells

MTT assay was performed to assess the viability of breast cancer (MDA-MB-231), cervical cancer (SiHa), and noncancerous human embryonic kidney (HEK-293) cells. The assay is based on cellular mitochondrial enzymes converting yellow-colored MTT to violet-colored formazan crystals. Interestingly, as shown in Figure **6.7 a** and **6.7 b**, ARCD and ARCCD showed anticancer efficacy by inhibiting the viability of breast cancer cells with half-maximum inhibitory concentrations (IC_{50}) of 507.2 µg/mL and 3002 µg/mL, respectively, for up to 48 hours. ARCD and ARCCD also inhibited cervical cancer cell proliferation for up to 48 hours, with half-maximum inhibitory concentrations (IC_{50}) of 755.1 µg/mL and 4738 µg/mL, respectively. However, both ARCD and ARCCD were harmless to HEK-293 cells, with the viability of over 90%, showing that ARCD and ARCCD had specificity toward cancerous cells only. The percent cell viability was calculated against various concentrations of ARCD and ARCCD, and the results revealed that CNDs has excellent inhibition efficiency for breast cancer MDA-MB-11 cells.

Phase-contrast microscopic pictures of HEK-293 and MDA-MB-231 cells treated with different amounts of ARCD and ARCCD were captured at 10X magnification, as shown in Figure **6.8**. In HEK-293 cells, no morphological alterations were observed; however, ARCD and ARCCD induced morphological changes such as detachment from the monolayer surface, abnormal cell shape, and a decrease in the number of viable cells in treated cells.

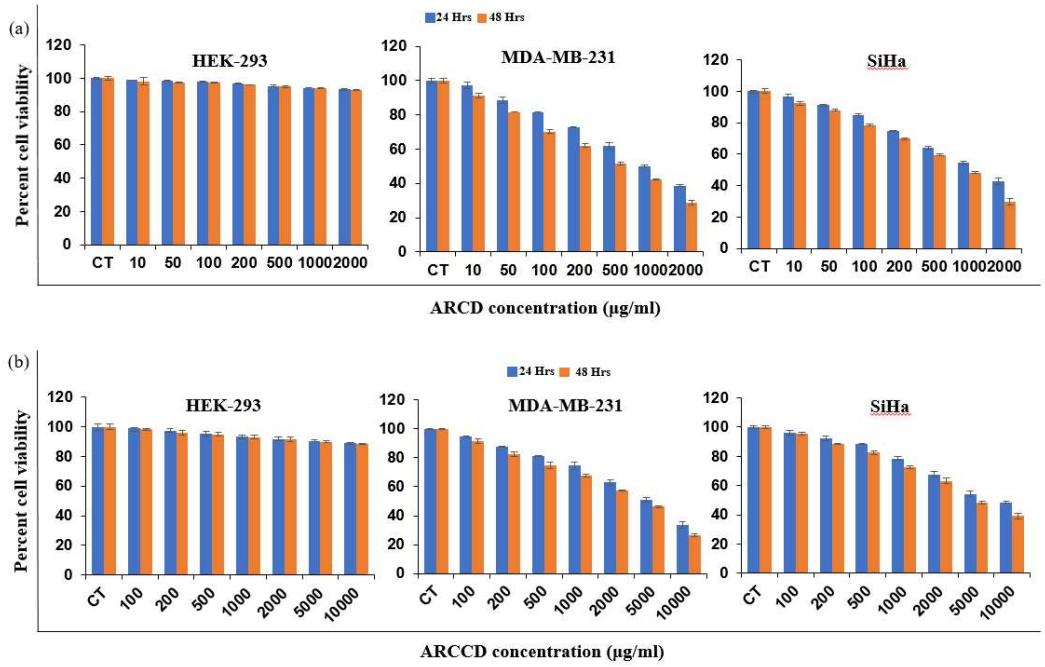

Figure 6.7. [a] and [b] Dose and time-dependent effect of ARCD and ARCCD on the proliferation of HEK-293, MDA-MB-231 and SiHa cell lines.

Cellular uptake studies

The majority of the CNDs were found in the nucleus of the cells, indicating that they entered the cells quickly via receptor-mediated or non-receptor-mediated endocytosis [Nel *et al.,* 2009, Song *et al.,* 2012]. DAPI labelling was used to observe morphological changes in the cell nucleus under a fluorescence microscope at a

magnification of 20X, as shown in Figure **6.9**. Round and oval-shaped nuclei were found in normal cells; however, nuclear fragmentation with nuclear apoptotic bodies and membrane blebbing were observed in ARCD and ARCCD-treated cells.

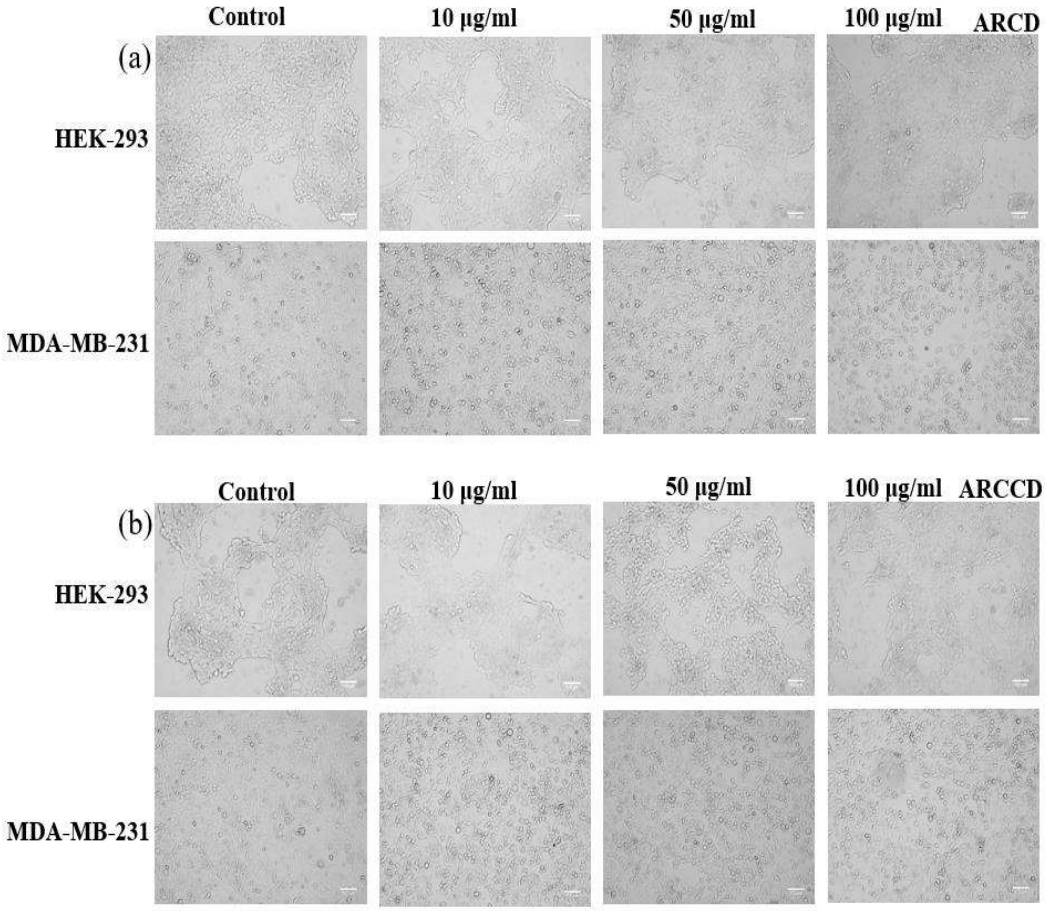

Figure 6.8. The phase contrast microscopic images of HEK-293 and MDA-MB-231 cells treated with various concentrations of [a] ARCD and [b] ARCCD at 10X magnification.

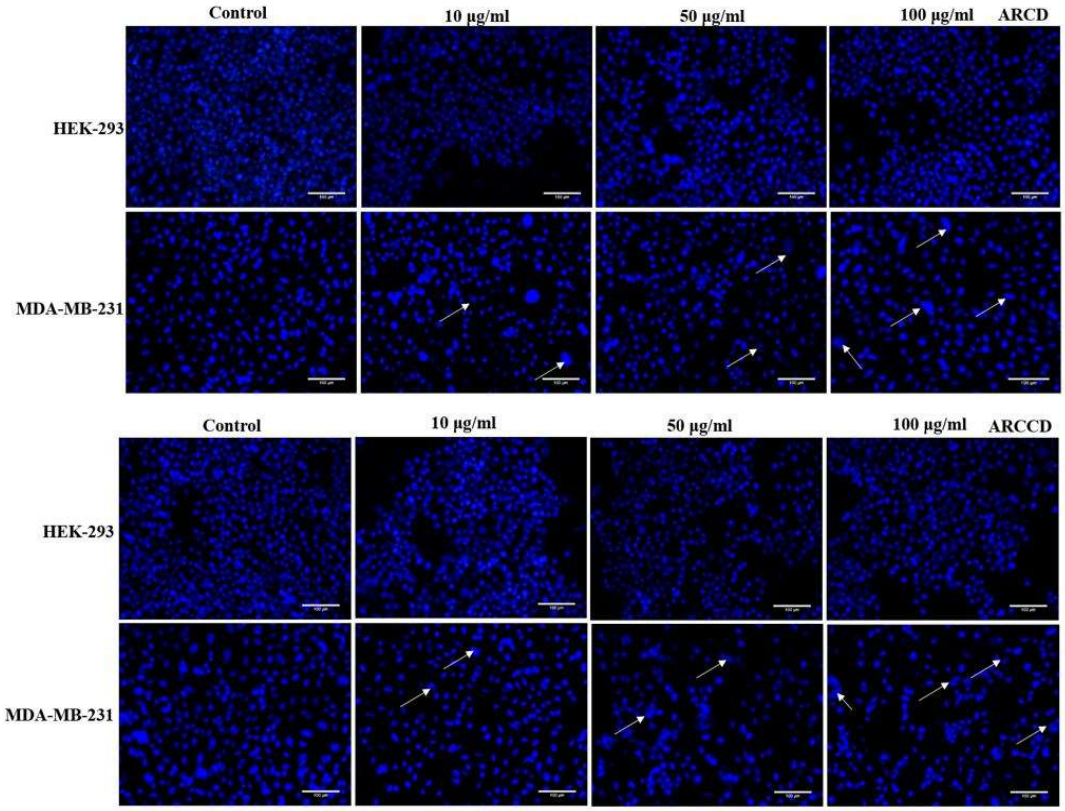

Figure 6.9. FL microscopic images of control and treated cells after DAPI staining with various concentrations of [a] ARCD and [b] ARCCD at 20X magnification. Scale: 100µm.

Western blot assay

Due to their small size and larger surface area, CNDs can enter cancerous cells through the EPR effect; hence it can also inhibit the growth of cancerous cells [Wang *et al.,* 2017]. Apoptosis is a form of programmed cell death regulated by the balance between pro-survival and pro-apoptotic Bcl-2 protein family members. Evasion of apoptosis is a hallmark of cancer that arises when this balance is tipped in favour of survival [Dadsena *et al.,* 2021]. Apoptosis has been regarded as a preferred route of anticancer action, and much work is being put into developing prospective drugs that can induce apoptosis in malignant cells.

As a result, we used some apoptosis-related parameters to explore the apoptotic potentials of CNDs on the most susceptible cell lines, i.e., MDA-MB-231 cells [Limner *et al.,* 2002]. Western blotting was performed to examine the expression pattern of proteins Bax and Bcl-2 involved in apoptosis. As shown in Figure **6.10**, ARCD and ARCCD both upregulated the expression level of the pro-apoptotic molecule Bax while downregulated the anti-apoptotic molecule Bcl-2. Therefore, these findings suggested that ARCD and ARCCD may serve crucial roles during the progression of cell apoptosis.

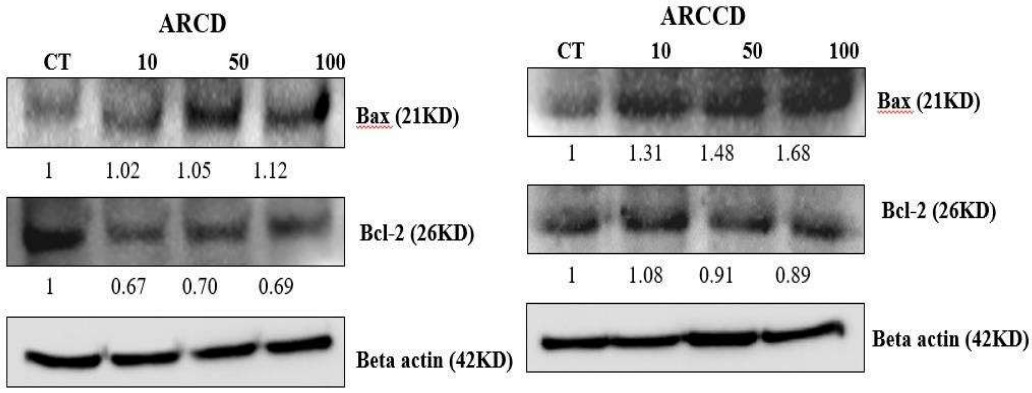

Figure 6.10. Immunoblotting was performed to examine the expression pattern of proteins involved in apoptosis.

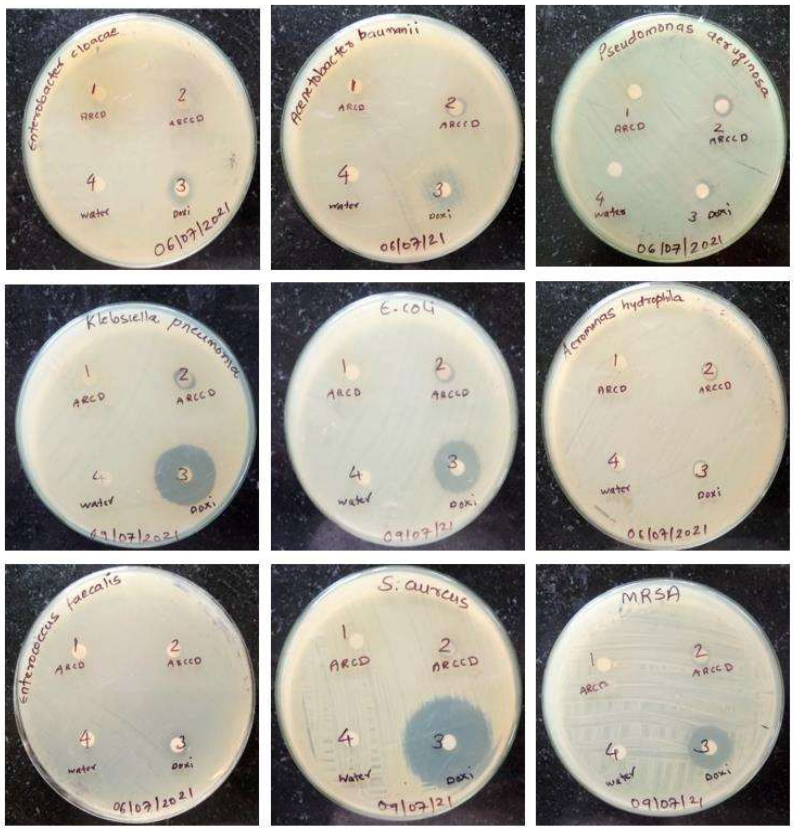

Figure 6.11. Anti-bacterial assay against clinically isolated multi-drug resistant strains with doxyclycline (positive control) and water (negative control).

6.3.5.3 Viability studies using MDR bacterial strains

The antibacterial activity of ARCD and ARCCD against nine clinically isolated MDR bacterial strains was studied in this study, as shown in Figure **6.11**. *Enterobacter cloacae* (G-), *Acinetobacter baumannii* (G-), *Escherichia coli* (G-), *Klebsiella pneumoniae* (G-), *Pseudomonas aeruginosa* (-), *Aeromonas hydrophila* (G-), *Staphylococcus aureus* (G+), *Enterococcus faecalis* (G+), and Methicillin-Resistant *Staphylococcus Aureus* (G+). The antibacterial activity of ARCD and ARCCD was investigated using the disc diffusion method with minor modifications. The zones of growth inhibition of *A. baumannii*, E. coli, *P. aeruginosa*, *K. pneumoniae*, and *A.*

hydrophila cells were observed surrounding the discs treated with 20 µL of 40 mg/mL ARCCD.

The observed growth inhibition zone of *P. aeruginosa*, *K. pneumonia*, *A. baumannii*, *E. coli*, and *A. hydrophila* for discs containing ARCCD was 9.2 mm, 9.1 mm, 8.6 mm, 7.3 mm, and 7.0 mm, respectively (Table **6.1**). These findings revealed that ARCCD is more effective than ARCD at inhibiting microbial growth. CNDs can breach the membrane or release free radicals and oxidizing species that cause bacterial cells to die owing to their high surface-to-volume ratio [Hajipour *et al.,* 2012]. This research lays the groundwork for the development of ARCCD as an antibacterial therapeutic, but more in-depth in-vivo research is required.

ARCD, on the other hand, showed no zone of inhibition compared to doxycycline, which was used as a positive control. The experiments were carried out in triplicates. These findings show that the ARCD is biocompatible in bacterial cells, indicating that it could be used in microbiology research and bacterial bio-imaging. It is worth noting that ARCCD only inhibits the growth of gram-negative bacteria and does not affect the growth of gram-positive bacteria. This could be due to a thick peptidoglycan layer and teichoic acids in gram-positive bacteria, preventing CNDs from entering the bacteria [Wang *et al.,* 2021].

Table 6.1. Table showing zones of inhibition.

Bacterial strain	**Average radial diameter of zone of growth inhibition (in mm)**			
	ARCD	ARCCD	Dox	DW
Gram negative				
Enterobacter cloacae	-	-	8±0.9	-
Acinetobacter baumannii	-	8±0.6	15±0.1	-
Pseudomonas aeruginosa	-	9±0.2	12±0.4	-
Escherichia coli	-	7±0.3	18±0.7	-
Klebsiella pneumonia	-	9±0.5	24±0.1	-
Aeromonas hydrophila	-	7±0.5	7±0.2	-
Gram positive				
Enterococcus faecalis	-	-	9±0.3	-
Staphylococcus aureus	-	-	34±0.5	-
Methicillin Rs. S. Aureus	-	-	10±0.4	-

(Data was represented as mean± SD)

6.3.5.4 Radical scavenging potential using DPPH assay

DPPH assay investigated the dose-dependent radical scavenging potential of CNDs at various concentrations. The deep violet color solution changed its color to pale yellow upon forming a stable DPPH-H complex [Mishra *et al.,* 2012]. With an increase in the ARCD and ARCCD concentrations, DPPH absorbance decreased significantly. The IC_{50} value for ARCD and ARCCD was 180.73 µg/mL and 253.02 µg/mL, respectively.

6.3.5.5 In-vivo toxicity evaluation in swiss albino mice

The results showed no evident differences between the ARCD and ARCCD groups. Statistically insignificant ($p > 0.05$) differences were observed on day 14 of the treatment in any experimental groups; this could be due to the body's immunological regulation. All biochemical assay values were within normal ranges.

Peripheral blood was collected from mice post-treatment for hematological toxicity determination and subjected to several hematological parameters evaluation. All the treatment groups and the normal control group's values were within the normal range. In addition, biochemical parameters (Table **6.2**) such as alanine aminotransferase (ALT), creatinine (CRE), aspartate transaminase (AST), alkaline phosphatase (ALP), blood urea nitrogen (BUN), total bilirubin (TB), cholesterol, and creatine phosphokinase (CPK) were also analyzed to measure organ toxicity as per standard protocols. Biochemical indicators were also within normal limits, showing that the mice were not harmed by delivering ARCD and ARCCD nanoparticles.

Table 6.2. Biochemical parameters of mice treated with CNDs and Control groups.

Parameters	***Control***	***Group I***	***Group II***	***Group III***	***Group IV***
ALP (U/L)	105.13± 5.57	95.36± 1.88	103.66± 2.28	104.33± 4.85	106.4± 2.20
AST(U/L)	134.46± 3.80	145.36± 4.36	145.3± 3.55	149.7± 2.57	150.5 ±3.93
ALT(U/L)	51.6± 1.75	55.03± 4.32	56.7± 1.15	46.73± 6.90	52.13± 3.57
Creatinine (mg/dL)	0.23± 0.02	0.22± 0.02	0.21± 0.01	0.23± 0.02	0.21± 0.01
Urea (mg/dL)	40.52± 3.86	43.11± 3.25	47.33± 2.14	50.59± 4.88	50.34± 3.57
Cholesterol (mg/dL)	103± 5.09	103.33± 4.18	105.33± 5.24	103.33± 5.79	109.33± 7.93
Tryglyceride (mg/dL)	106.53± 3.61	114.87± 6.50	134.10± 4.45	122. ± 7.11	121.19± 4.35
Protein (g/dL)	6.39± 0.54	6.58± 0.54	6.89± 0.69	6.41± 0.83	6.46± 0.48
Glucose (mg/dL)	140.93± 9.12	141.23± 2.37	162.76± 4.19	152.6± 5.58	142.56± 4.69
CPK Total(U/L)	96.33± 5.24	100± 6.68	104.33± 3.29	95.66± 6.23	98 ± 5.71

(Data was represented as mean± SD)

Table 6.3. Hematological parameters of mice treated with CNDs and control groups.

Parameters	Control	Group I	Group II	Group III	Group IV
WBC (10^3/μL)	36.54±2.35	35.55±2.88	35.56±1.17	35.33±2.8	34.08±1.28
HGB (g/dL)	11.74±0.64	11.87±0.57	11.29±0.20	12.24±0.74	11.52±0.24
RBC (10^6/μL)	8.27±0.33	8.20±0.19	8.30±0.31	7.91±0.22	8.07±0.35
HCT (%)	36.12±1.40	37.57±1.15	37.51±1.49	35.62±2.49	37.94±1.72
MCV (fL)	45.69±1.03	46.31±0.84	46.13±2.41	46.21±0.66	46.24±2.31
MCH(pg)	14.38±0.21	14.63±0.35	14.46±0.22	14.47±0.28	14.45±0.26
NEUT (%)	55.80±2.94	51.68±5.73	54.47±3.89	52.63±3.09	52.18±1.55
LYM (%)	41.12±5.61	39.44±2.21	42.25±3.53	41.5±3.81	39.85±4.94
MONO (%)	3.76±0.33	3.78±0.15	3.86±0.17	4.04±0.29	3.79±0.13
EO (%)	0.80±0.03	0.84±0.01	0.85±0.01	0.84±0.03	0.82±0.01
BASO (%)	0.02±0.02	0.04±0.02	0.01±0.02	0.06±0.01	0.05±0.01

(Data was represented as mean± SD)

The histological investigation determined the microscopic interactions between CNDs and biological tissues. There were no evident histopathological changes in the heart, brain, kidney, spleen, lung, or liver observed compared to the control group. A histopathological examination revealed no signs of severe toxicity. These alterations could be attributable to environmental causes, like the mice in the control group exhibit

comparable symptoms. The cells and structure of these organs' samples were confirmed to be normal, and no specific lesion that differed from the control group was observed. The vital organs' H&E staining revealed the same characteristics as control sections. On histological evaluation, the heart, kidney, brain, spleen, lung, and liver did not reveal any signs of toxicity, as shown in Figure **6.12**. In the test groups, no evident histological abnormalities or lesions were seen. The test group's cardiac muscle fibres were uniform and normal in shape and size. The hepatocytes in the liver samples were normal, and no evidence of inflammation was seen. In the renal portion, the glomerulus structure was normal in texture. There was no evidence of necrosis in any of the histopathological samples examined. There was no steatosis, necrosis, or hydropic degeneration in the exposed hepatic sections. The liver lobule structure was normal, with only a few collagen fibres in the central vein and portal area. The red and white pulps were clear, and the splenic capsule was complete. The architecture of the lungs was normal, and no inflammation was discovered. The glomerular structure may be seen clearly in portions of the kidneys. Every other day, body weights were measured, and there were no differences between the experimental and control groups.

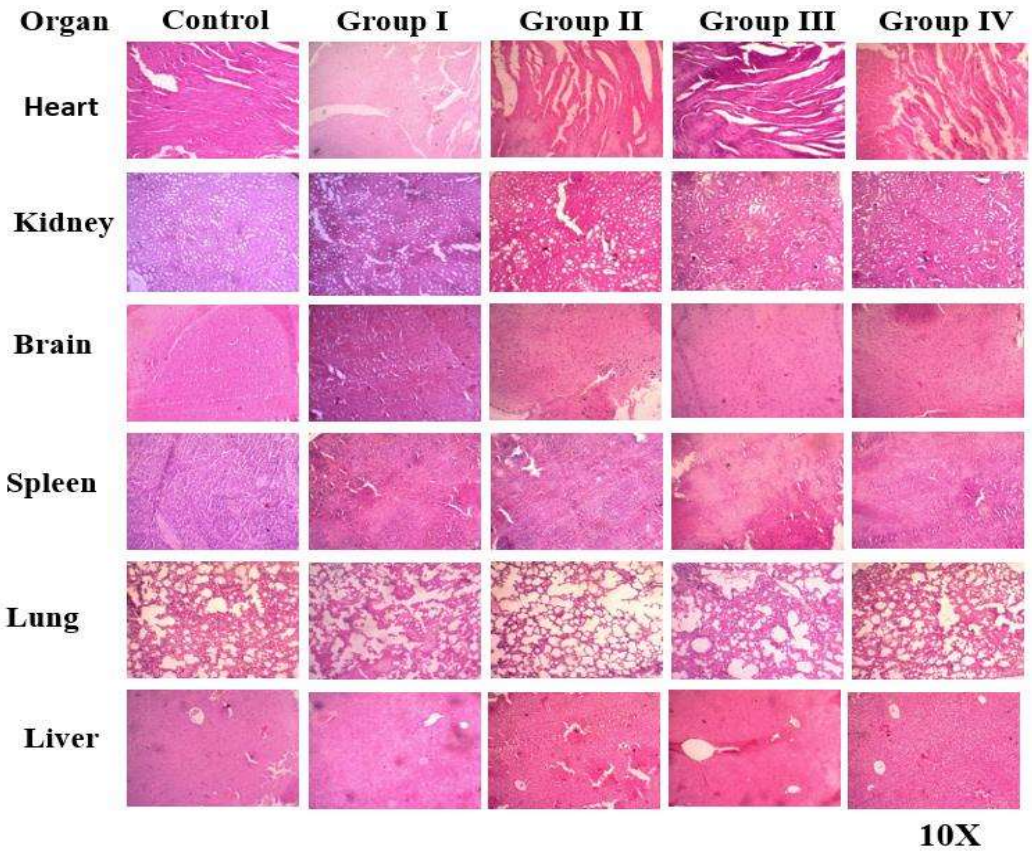

Figure 6.12. Histopathology of different mice organs treated with CNDs and control. Group I: ARCD@1mg/kg BW, Group II: ARCD@2mg/kg BW, Group III: ARCCD@4mg/kg BW , Group IV: ARCCD@8mg/kg BW.

6.4 Conclusion

In the present study, fluorescent CNDs were successfully synthesized from the *Asparagus racemosus* roots and other surfaces passivated with carrageenan and PEI via green synthesis hydrothermal treatment. Upon surface passivation of ARCD, the quantum yield improved from 2.46% to 4.47%. ARCD and ARCCD were employed as the fluorescent nano-probe for As^{3+} and Ag^{+} ion detection with a detection limit of 0.227 µM and 0.052 µM, respectively, lower than the maximum permissible level for these heavy metals in drinking water. By assessing the quantity of these heavy metals, we envisage that these CNDs can be used to assess the safety and quality of drinking water. No significant cytotoxicity was observed in the Normal Kidney (HEK 293) cell line, indicating specific cytotoxicity of the developed CNDs towards cancerous cells. Both ARCD and ARCCD upregulated the expression of pro-apoptotic molecule Bax while downregulated the expression of anti-apoptotic molecule Bcl-2, indicating crucial roles of these CNDs in the progression of cell apoptosis. Moreover, no hematological and biochemical toxicity was observed in swiss albino mice, which illustrates the potential of these CNDs as safe and effective. The obtained findings validated the potential of CNDs for biomedical and environmental analysis.